

# The Effects of Metastable Solvated Ions on Electro spray Ion Thruster Efficiency

IEPC-2015-179/ISTS-2015-b-179

*Presented at Joint Conference of 30th International Symposium on Space Technology and Science,  
34th International Electric Propulsion Conference and 6th Nano-satellite Symposium  
Hyogo-Kobe, Japan  
July 4–10, 2015*

Catherine E. Miller\* and Paulo C. Lozano†  
*Massachusetts Institute of Technology, Cambridge, MA, 02139, USA*

Ionic liquid ion sources use ionic liquids to produce beams of pure and solvated ions. Past experiments have shown that solvated ions are metastable and can fragment into lighter ions and neutral solvated species. This has an important effect on the propulsive efficiency of ion electro spray thrusters, which use arrays of ionic liquid ion sources to produce thrust. It has been hypothesized that the molecular complexity of the ions in ionic liquids plays an important role in the stability of solvated species. Past work indicates that the stability of solvated ions increases with the complexity of the ions. In this work, retarding potential analysis and time of flight mass spectrometry are used to evaluate the dependence of fragmentation on the molecular complexity. It was found that the stability of solvated ions tends to increase with increasing molecular complexity, with a few exceptions. This work is not sufficient to determine the validity of the hypothesis and only provides an indication of the trends. The limitations of the detectors may be responsible for the outliers and further work is required to evaluate the hypothesis with more confidence.

## Nomenclature

$d$	= flight distance
$f_0$	= monomer current fraction
$f_f$	= fragmented dimer fraction
$I_T$	= beam current
$\dot{m}$	= mass flow rate
$m_i$	= mass of ion
$m_{pi}$	= mass of parent ion
$\eta_E$	= energy efficiency
$\eta_i$	= ionization efficiency
$\eta_p$	= polydispersive efficiency
$\eta_t$	= transmission efficiency
$\eta_T$	= thruster efficiency
$\eta_\theta$	= angular efficiency
$V_0$	= extraction potential
$V_B$	= potential at which fragmentation occurs
$v_i$	= velocity of ion
$\xi$	= ratio of dimer to monomer charge to mass ratios

---

\*Graduate Student, Department of Aeronautics and Astronautics, and millerce@mit.edu.

†Associate Professor, Department of Aeronautics and Astronautics, and plozano@mit.edu.

## I. Introduction

ION electrospray thrusters use ionic liquids, or molten salts, as propellant. Ionic liquids consist entirely of positive and negative ions. Thus they have moderate conductivities and negligible vapor pressures.<sup>1</sup> Ions can be evaporated from the surface of these liquids through the application of a sufficiently strong electric field.<sup>1</sup> Thrust is produced by accelerating the evaporated ions with the electric field.

The electric field strength required for ion evaporation is typically about  $1 \text{ V/nm}$ ,<sup>2</sup> which requires the use of sharp emitter geometries to enhance the local electric field. A schematic of a single emitter ionic liquid ion source (ILIS) is shown in Fig. 1. The emitter in Fig. 1 consists of an externally wetted tungsten

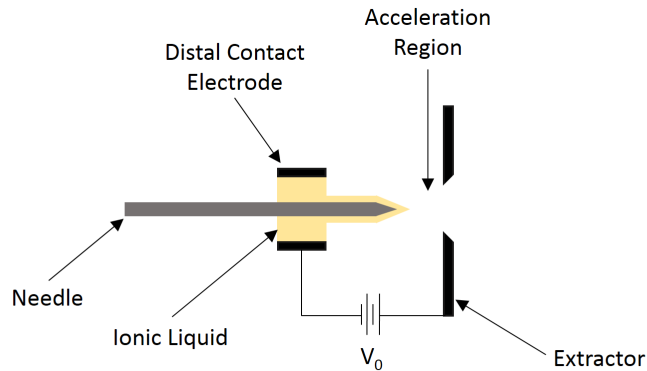


Figure 1. Single Emitter Ionic Liquid Ion Source.<sup>3</sup>

needle, a distal contact electrode that is also a reservoir for the ionic liquid, and a metal extraction plate. A potential  $V_0$ , typically 1-2 kV, is applied between the distal electrode and the extractor plate. This stresses the surface of the liquid at the tip of the needle, resulting in the formation of a Taylor cone.<sup>4</sup> Taylor cones are a result of the surface tension pressure of the liquid being balanced with the electrostatic pressure of the applied field.<sup>1</sup> Taylor cones are sharper than the needle apex, which allows the electric field to reach the required strength for ion evaporation at the tip of the cone. Ions are evaporated from a very localized region at the cone tip and are accelerated through the hole in the extractor plate, producing an ion beam.

## II. The Effect of Ion Beam Composition on Thruster Efficiency

Ionic liquids consist of cations, usually a heavy organic molecule, and anions, usually an inorganic molecule or a single atom.<sup>2</sup> Fig. 2 shows the molecular structure of EMI- $\text{BF}_4$ , which is one of the most well tested ionic liquids in ionic liquid ion sources.<sup>1,5,6</sup>

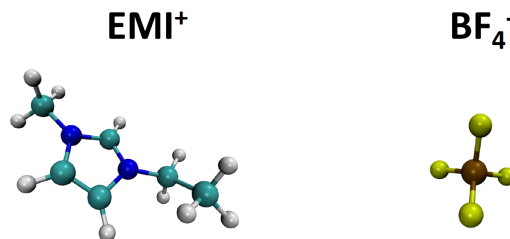


Figure 2. Molecular Structure of EMI- $\text{BF}_4$ .<sup>2,3</sup>

ILIS beams contain several different types of ions, such as monomers, which are single ions. For EMI- $\text{BF}_4$  in the positive mode, the monomers are EMI<sup>+</sup> ions. In the negative mode, the monomers are BF<sub>4</sub><sup>-</sup> ions. It is well known that solvated ions are also present in ILIS beams.<sup>1</sup> Solvated ions are single ions attached to at

least one cation-anion pair. Cation-anion pairs are called neutrals since they have zero net charge. A dimer is a single ion attached to one neutral and a trimer is a single ion attached to two neutrals. The monomer and dimer for EMI-BF<sub>4</sub> in the positive mode are shown in Fig. 3.

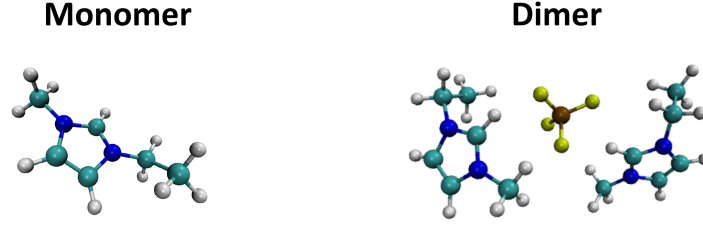


Figure 3. Molecular Structure of EMI-BF<sub>4</sub> Positive Monomer and Dimer.<sup>2,3</sup>

The presence of solvated species has a negative effect on the thruster efficiency. The efficiency of an electro spray thruster can be expressed by Eq. (1) shown below:<sup>7</sup>

$$\eta_T = \eta_i \eta_t^2 \eta_\theta \eta_E \eta_p \quad (1)$$

$\eta_i$  is the ionization efficiency, which accounts for the loss of propellant through the emission of neutral species; the ionization efficiency is 100% for ILIS because the ions are already available in the liquid.<sup>7</sup>  $\eta_t$  is the transmission efficiency, which accounts for the interception of the ion beam on the extractor grid.<sup>7</sup> With good alignment of the tip and extractor hole, the transmission efficiency should be nearly 100%.  $\eta_\theta$  is the angular efficiency, which penalizes divergent ion beams.<sup>7</sup> ILIS beams typically have a half angle spread of 18°,<sup>1</sup> which results in an angular efficiency of about 98%.<sup>7</sup>  $\eta_E$  is the energy efficiency, which is about 98% for ILIS.<sup>7</sup> When ions are extracted from the liquid surface, there is a small voltage loss which results in less potential available for accelerating the ions.<sup>7,8</sup> Finally  $\eta_p$  is the polydispersive efficiency which accounts for propulsive losses incurred by accelerating beam constituents to different velocities.<sup>2,7</sup>

Maximum propulsive efficiency occurs when all particles in a stream of exhaust are travelling at the same velocity.<sup>2</sup> When there is a spread in particle velocities, the propulsive efficiency is decreased due to the polydispersity.<sup>2</sup> In ILIS, the monomers and dimers exit the thruster at different velocities. This occurs because they have different masses. Eq. (2) shows the velocity,  $v_i$ , of an ion of mass  $m_i$  and charge  $q_i$  that has been accelerated through a potential  $V_0$ .

$$v_i = \sqrt{\frac{2q_i V_0}{m_i}} \quad (2)$$

Ions with the same charge that are accelerated through the same electrostatic potential will have different velocities if they have different masses. The polydispersive efficiency for an ion beam is given by Eq. (3):<sup>2</sup>

$$\eta_p = \frac{(\sum_i \dot{m}_i v_i)^2}{2\dot{m}_T I_T V_0} \quad (3)$$

where  $\dot{m}_i$  is the mass flow rate of the  $i^{th}$  species of ion,  $v_i$  is the velocity of the  $i^{th}$  species of ion,  $\dot{m}_T$  is the total mass flow rate,  $I_T$  is the total beam current, and  $V_0$  is the accelerating potential.<sup>2</sup> This is simply the ratio of the kinetic jet power of the ion beam to the electric power used to accelerate the ions.

For a beam of monomers and dimers, the polydispersive efficiency is given by Eq. (4):<sup>2</sup>

$$\eta_p = \frac{[1 + (\sqrt{\xi} - 1)f_0]^2}{1 + (\xi - 1)f_0} \quad (4)$$

Where  $\eta_p$  is the polydispersive efficiency,  $\xi$  is the charge to mass ratio of the dimer divided by the charge to mass ratio of the monomer, and  $f_0$  is the monomer current fraction.<sup>2</sup> Fig. 4 shows the polydispersive efficiency as a function of the monomer current fraction for EMI-BF<sub>4</sub>. The polydispersive efficiency is 1 for when the beam consists of a single species. The minimum efficiency is given by Eq. (5) and the corresponding monomer fraction at the minimum is given by Eq. (6).

$$\eta_{p,min} = \frac{1}{\sqrt{\xi}} \left( 1 + \frac{(\sqrt{\xi} - 1)^2}{\xi - 1} \right)^2 \quad (5)$$

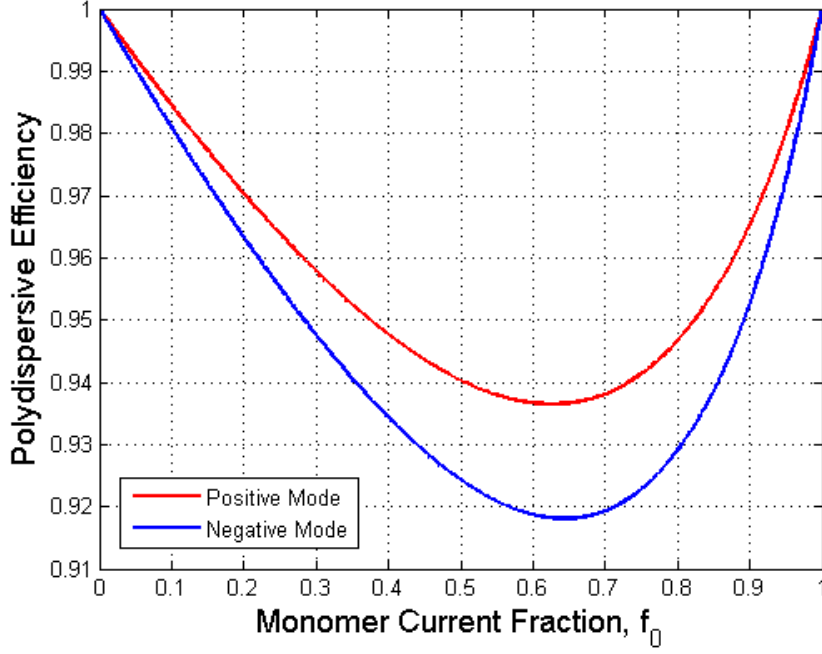


Figure 4. Polydispersive Efficiency for EMI-BF<sub>4</sub>.<sup>3</sup>

$$f_{0,min} = \frac{\sqrt{\xi} - 1}{\xi - 1} \quad (6)$$

The minimum polydispersive efficiency goes to zero as  $\xi$  goes to zero. This means that if the disparity between the masses of the dimer and monomer is very large, the efficiency will suffer more so than if the masses of the two species are similar.

It has been observed that solvated ions are metastable.<sup>2,8</sup> As an example, dimers fragment into monomers and neutrals. This process is called fragmentation and it can further decrease the polydispersive efficiency.<sup>2</sup> If fragmentation occurs outside of the thruster, the polydispersive efficiency is not affected because the ions are no longer being accelerated.<sup>2</sup> If fragmentation occurs within the acceleration region, the efficiency will be reduced because the ions are still being accelerated.<sup>2,7</sup> For example, if a dimer breaks up into a monomer and a neutral in the acceleration region, the monomer will continue to be accelerated. The neutral cannot be further accelerated and it will exit the thruster at a slower velocity than that of an unfragmented dimer. The monomer will be accelerated to a velocity faster than that of an unfragmented dimer, but slower than that of a monomer that was directly emitted from the liquid surface. The final velocities of the fragments will depend on the local value of the electric potential where the parent ion broke up, thus the fragments will have a spread in velocities. This extra spread in velocities reduces the polydispersive efficiency.

Eq (4) can be modified to include the fragmentation of dimers into monomers, the result is shown in Eq. (7):<sup>2</sup>

$$\eta_p = \frac{[1 + (\sqrt{\xi} - 1)f_0 + \frac{1}{3}f_f(2\sqrt{\xi}\frac{1-\sqrt{\xi}}{1-\xi} - 1)]^2}{1 + (\xi - 1)f_0} \quad (7)$$

where  $f_f$  is the current fraction of dimers that fragment into monomers.<sup>2</sup> A critical assumption was made in the formulation of Eq. (7). It was assumed that the fragmentation of dimers into monomers occurs uniformly with respect to the acceleration potential.<sup>2</sup> While this assumption has not been experimentally confirmed, the results of past experiments seem to indicate that it is a reasonable assumption.<sup>2</sup> The effect of fragmentation on the polydispersive efficiency for EMI-BF<sub>4</sub> in the positive mode is shown in Fig. 5.

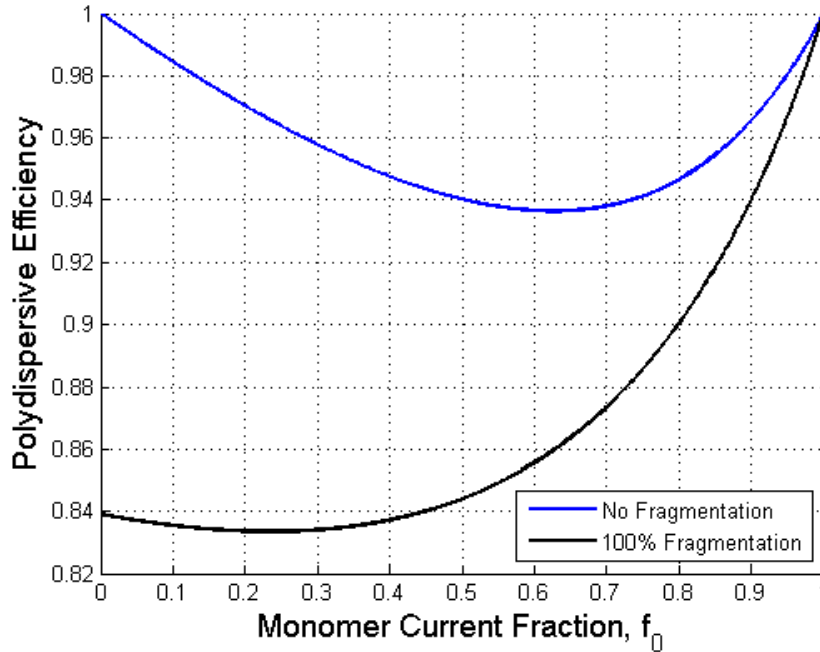


Figure 5. Polydispersive Efficiency for EMI-BF<sub>4</sub> With Fragmentation.<sup>3</sup>

The efficiency is still 1 for a beam entirely composed of monomers, but with the added effect of fragmentation, a beam of dimers does not necessarily result in an efficiency of 1. The decrease in efficiency is substantial, which makes solvated ion fragmentation an important area of study.

### III. The Effect of Ion Complexity on Fragmentation

From past experiments, it has been shown that different ionic liquids show different amounts of fragmentation.<sup>2</sup> The fraction of current that comes from fragments can be determined by measuring the energy of the beam.<sup>3</sup> If the beam consists of only monomers and dimers that do not break up, the beam should be monoenergetic with an energy of  $V_0$  in eV's.<sup>2,3</sup> Fragmented species always have less energy than the acceleration potential; therefore the low energy components of the beam energy distribution correspond to the fragmented species.<sup>2,3,8</sup> Table 1 shows the results of past experiments, which used beam energy measurements to determine the fragmentation fractions.

Table 1. Summary of Experimental Results (Negative Mode).<sup>3,9</sup>

	Fragmentation Before Emission	Total Fragmentation
BMI-I	50%	65%
EMI-BF <sub>4</sub>	12%	51%
EMI-Im	3%	11%

The ionic liquids used in past experiments are imidazolium based. EMI<sup>+</sup> and BMI<sup>+</sup> have very similar molecular structure since they both contain an imidazolium ring. BMI<sup>+</sup> has a longer carbon chain, an extra two carbon atoms and four hydrogen atoms, than EMI<sup>+</sup>. Since EMI<sup>+</sup> and BMI<sup>+</sup> only differ by a few atoms, the major difference between the liquids are the anions. The molecular structure of the anions is shown in Fig. 6.

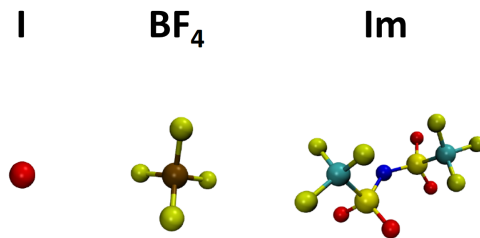


Figure 6. Molecular Structure of Anions.<sup>2,3</sup>

By comparing the molecular complexity of the anions to the fragmentation fractions in Table 1, it can be seen that the fragmentation fraction increases with decreasing molecular complexity.<sup>2</sup> Iodine is a single atom and it has the highest fragmentation fraction. Im has the most atoms and it fragments the least.  $\text{BF}_4$  has five atoms, which is more than iodine but less than Im, and it fragments less than iodine but more than Im. It is very important to note that these experiments were conducted using different experimental apparatuses and source operation conditions.<sup>2,6,8,10</sup> Therefore strong conclusions should not be made by the comparison of these past results.<sup>2</sup> This motivates further study under controlled conditions so that each liquid is tested on an equal basis.

Molecular dynamics simulations have been conducted to test the stability of solvated species.<sup>2</sup> Negative dimers of  $\text{EMI}^+$  based ionic liquids were simulated 10,000 times to see if they broke up during a set amount of time in the presence of a particular electric field strength.<sup>2</sup> It was found that the fragmentation percentage decreased with increasing number of atoms in the negative dimer, which increases with the molecular complexity of the anion.<sup>2</sup> Therefore the molecular dynamics simulations support the past experimental observations.<sup>2</sup>

The hypothesis for this work is that solvated ion stability increases with increasing molecular complexity, which makes physical sense. The ion extraction process imparts excess energy to the solvated species, which can cause the individual ions to stretch back and forth.<sup>2,3</sup> If they stretch too far apart, the solvated ion could break up.<sup>2,3</sup> This excess energy can be redistributed throughout the many bonds of complex molecules.<sup>2,3</sup> Therefore there is less energy that can stretch the individual ions apart, and the complex ions should fragment less frequently.<sup>2,3</sup>

## IV. Experimental Methods

In this work the beam composition and fragmentation fractions were measured for different ionic liquids under controlled conditions. The ion source is a single, externally wetted tungsten needle, like that depicted in Fig. 1. The radius of curvature of the needle used in these experiments is approximately 20 micrometers.<sup>3</sup> Two measurement techniques were employed: retarding potential analysis (RPA), and time of flight mass spectrometry (TOF). Retarding potential analysis gives the fragmentation current fractions both in the acceleration region and in field-free space.<sup>2,3</sup> Time of flight mass spectrometry provides the beam composition and the current fraction of fragmented species that broke up in the acceleration region.<sup>3</sup>

The configuration of the ion source is the same for all experiments. The externally wetted needle and the distal contact liquid reservoir are mounted to a boron nitride block.<sup>3</sup> A ceramic resistive heater and a K-type thermocouple are also mounted to the boron nitride block.<sup>3</sup> The temperature of the liquid is kept constant using an Arduino UNO to control the heater circuit.<sup>3</sup> The RPA and TOF measurements were taken at a set range of temperatures and voltages to ensure that the liquids are compared on an equal basis.

### A. Retarding Potential Analysis

A retarding potential analyzer uses semi-transparent grids biased to high voltages.<sup>2,3,8</sup> An RPA consists of a set of grids placed in front of a current collecting surface. Fig. 7 shows a diagram of the RPA used in this work. The first grid is placed behind an aperture, both of which are grounded; the aperture is used to help reduce beam spreading effects in the RPA curves by sampling a smaller solid angle of the beam.<sup>3</sup> The middle set of grids consists of four 90% transparent grids made from parallel tungsten wires.<sup>8</sup> The orientation of a given grid is such that the direction of the tungsten wires of that grid is rotated  $90^\circ$

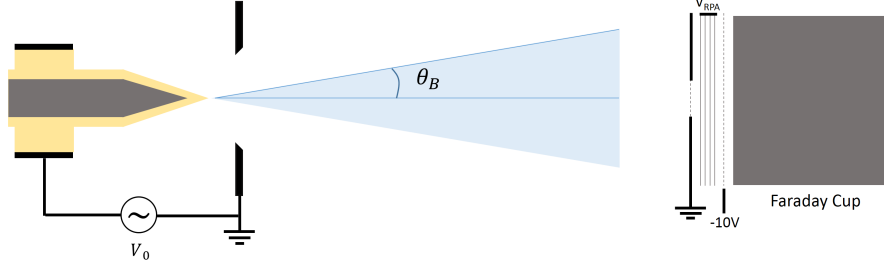


Figure 7. Retarding Potential Analyzer.<sup>3</sup>

from that of the grids adjacent to it.<sup>3</sup> The final grid before the Faraday cup is a coarse mesh grid that is biased to approximately -10V to suppress any secondary electrons that are created through the impacts of ions with the current collecting surface.<sup>3</sup> The distance between the extractor plate and the RPA entrance aperture is approximately 1 cm.<sup>3</sup> The retarding grids are varied from ground to approximately 1.5 times the accelerating potential  $V_0$ . If an ion has a kinetic energy equal to the retarding potential, in eV's, then that ion will be stopped and will not be collected by the Faraday cup.<sup>2,3</sup> Thus measuring the collected current as a function of the retarding potential yields the energy distribution of the beam.

The fragmentation features on the RPA curve depend on whether the solvated ions break up in field-free space or in the acceleration region.<sup>2,3</sup> If a solvated ion breaks up in field-free space, it is no longer being accelerated so it will have the same velocity as the solvated ion. Since the broken ion is lighter, it will have less kinetic energy than its parent solvated ion. The kinetic energy of a broken ion from a fragmentation event in field-free space is given by Eq. (8):<sup>3,8</sup>

$$K_{bi} = \frac{m_i}{m_{pi}} q_i V_0 \quad (8)$$

where  $K_{bi}$  is the kinetic energy of the broken ion,  $m_i$  is the mass of the broken ion,  $m_{pi}$  is the mass of the parent ion,  $q_i$  is the charge of the broken ion, and  $V_0$  is the accelerating potential.<sup>3</sup> For a given accelerating potential, this kinetic energy is a constant value that only depends on the masses of the parent and broken ions. Fragmentation in field-free space will appear as sharp steps in the current since the energy is the same for all broken ions of a given species that are created in field-free space.

When fragmentation occurs in the acceleration region, the broken ion continues to be accelerated to some final velocity. The kinetic energy of a broken ion from a fragmentation event in the acceleration region is given by Eq. (9):<sup>3,8</sup>

$$K_{bi} = q_i \left( \left( \frac{m_i}{m_{pi}} - 1 \right) V_B + V_0 \right) \quad (9)$$

Where  $K_{bi}$  is the kinetic energy of the broken ion,  $q_i$  is the charge of the ion,  $m_i$  is the mass of the broken ion,  $m_{pi}$  is the mass of the parent ion,  $V_B$  is the local value of the potential where the parent ion broke up, and  $V_0$  is the accelerating potential.<sup>3</sup> Fragmentation in the acceleration region produces broken ions with a spread in kinetic energies, therefore the RPA curves will have sloped features.<sup>2,3</sup> The features will be straight lines if the fragmentation in the acceleration region is uniform with respect to the accelerating potential.<sup>2,3</sup>

Fig. 8 a) shows a monoenergetic idealized RPA curve and b) and idealized RPA curve with fragmentation in both the acceleration region and in field-free space on the right. The straight steps in the RPA curve on the right side of Fig. 8 correspond to fragmentation in field-free space. The slopes are from uniform fragmentation in the acceleration region. By measuring the heights of the steps and slopes, the current fraction due to each type of fragmentation can be determined.

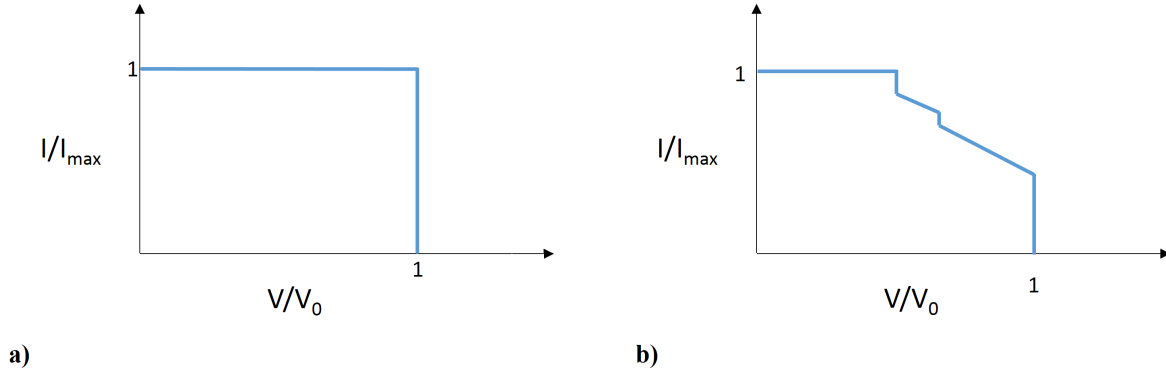


Figure 8. Idealized RPA Curves: a) Monoenergetic, b) Fragmentation.<sup>3</sup>

## B. Time of Flight Mass Spectrometry

Time of flight mass spectrometry yields the composition of the beam and the current fraction from fragmentation in the acceleration region.<sup>3</sup> Eq. (1) is the velocity of any ion that was not produced from a fragmentation event. It is clear that monomers are faster than dimers since the ion velocity decreases with the square root of the ion mass. If a detector is placed far from the ion source, each species of ion will take a certain amount of time to reach the detector based on the flight distance and the ion velocity. This is the basis of time of flight mass spectrometry, through which the masses of the ions can be determined by their flight times. Fragmentation results in ions with a spread in velocities, which are distinguishable from non-fragmented species in TOF measurements.<sup>3</sup>

A time of flight measurement system consists of a gate and a detector. The gate is used to interrupt the ion beam and the detector, placed far from the source, is used to measure the current as a function of time.<sup>3</sup> Fig. 9 shows a diagram of the time of flight detector used in this work. The gate is a simple electrostatic deflection gate that is pulsed on and off at a frequency of 500 Hz; the two deflector plates are biased to +950V and -950V respectively.<sup>3</sup> The current reaching the detector is very low since only a very small solid angle of the beam is sampled. In order to detect the fragmentation in the acceleration region, the

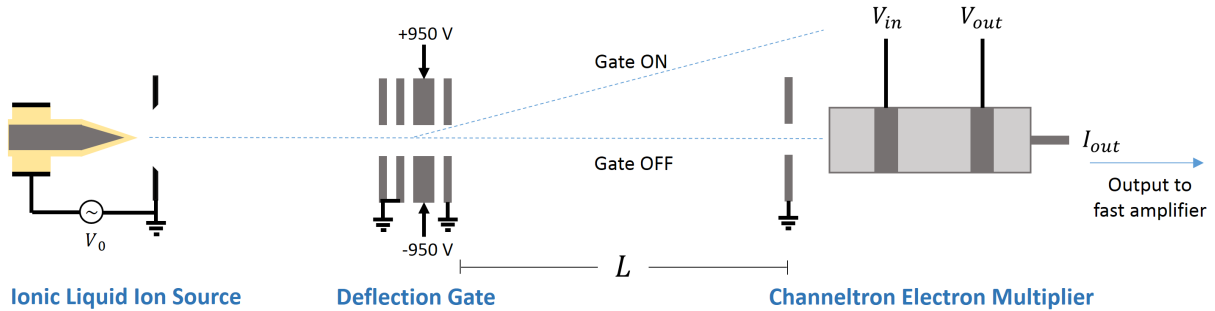


Figure 9. Time of Flight Detector.<sup>3</sup>

TOF detector must have a fast response time. The detector in this case is a Channeltron electron multiplier (Photonis Channeltron 5900 Magnum), which amplifies the measured current by  $10^5 - 10^8$ .<sup>3</sup> Channeltron electron multipliers (CEM) amplify the signal very quickly, so for the purposes of this work, they do not limit the electronic response time. Instead the non-inverting amplifier with gain used to amplify the CEM output signal is what limits the electronic response time to a few hundred nanoseconds.<sup>3</sup> The CEM signal needs to be amplified because the maximum output current is about 10 microamps.<sup>3</sup> The current signal is terminated through a 1 k $\Omega$  resistor and the voltage signal is amplified by a non-inverting op-amp with a gain of 50, resulting in a net amplifier gain of  $5 \times 10^4$ .<sup>3</sup> The output of the amplifier is measured using an

oscilloscope that is triggered to the gate pulses.

The flight time for an ion that was not produced from a fragmentation event is given by Eq. (10):<sup>3</sup>

$$t = d\sqrt{\frac{m_i}{2q_iV_0}} \quad (10)$$

where  $d$  is the flight distance, which is approximately 80 cm.<sup>3</sup> The flight time for a broken ion that was produced by fragmentation in the acceleration region is given by Eq. (11):<sup>3</sup>

$$t_{bi} = \frac{d}{\sqrt{\frac{2q_iV_0}{m_i} \left(1 - \frac{V_B}{V_0} \left(1 - \frac{m_i}{m_{pi}}\right)\right)}} \quad (11)$$

where  $V_B$  is the local value of the potential in the acceleration region where the solvated ion broke up. Fig. 10 shows idealized TOF measurements for a beam with only monomers and dimers without fragmentation in a) and with fragmentation in b). It was assumed that the fragmentation of dimers into monomers occurs uniformly with respect to the accelerating potential. The current fractions of each ion species can

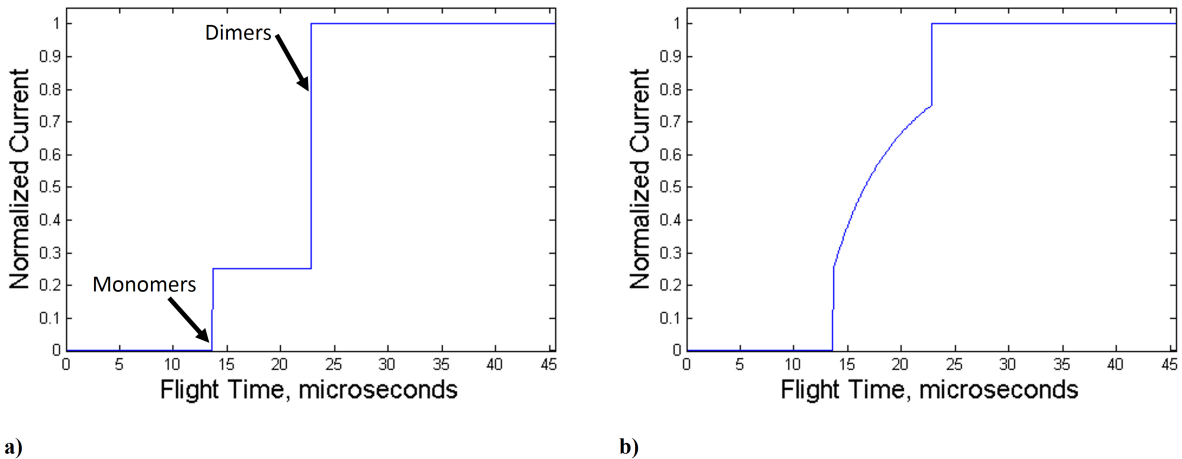


Figure 10. Idealized TOF Measurements: a) Monoenergetic, b) Fragmentation.

be determined from TOF measurements like the idealized ones in Fig. 10. The current fraction from fragmentation in the acceleration region can also be determined.<sup>3</sup> Additionally the distribution of break up with respect to the acceleration potential can be found by differentiating the TOF signal.<sup>3</sup> This can be used to determine if break up occurs uniformly with respect to the acceleration potential.<sup>3</sup>

## V. Results and Discussion

All ionic liquids were tested using the RPA and TOF apparatuses at four different temperatures: 30°C, 50°C, 70°C, and 90°C. Data was taken in 50 V steps over a voltages where the source emitted current in a stable and consistent manner.<sup>3</sup>

### A. Retarding Potential Analysis

The retarding grids were varied from ground to a few hundred volts beyond the source potential using a triangular waveform with a period of 5 seconds.<sup>3</sup> The RPA scan for a given voltage and temperature was averaged several times and then binned into 5 V intervals.<sup>3</sup> Unfortunately the RPA entrance aperture was not well aligned with the extractor aperture, which resulted in a lower than expected signal strength.<sup>3</sup> Additionally there was still significant beam spreading and some other anomalous features that may be a result of an electrostatic focusing effect from the retarding grids.<sup>3</sup> This made distinguishing subtle features like fragmentation in the acceleration region difficult. Therefore the only useful result from the RPA scans is

the current fraction due to the fragmentation of dimers into monomers in field-free space.<sup>3</sup> Fig. 11 shows an RPA scan for BMI-I at 70° and 1600 V. Note that 1600 V is the control signal for the high voltage amplifier; the applied voltage is typically about 10V-20V larger than the control signal,<sup>3</sup> but it is easier to refer to the control signal voltage because it is a round number. The blue horizontal lines show the measured step height for the fragmentation of a dimer into a monomer in field-free space. The black vertical line shows the energy of a monomer originating from a dimer that fragmented in field-free space, which is where the step should begin. The aforementioned anomalous features are evident in Fig. 11, namely the decreases in current. The step height relative to the total collected current was determined for all RPA scans.

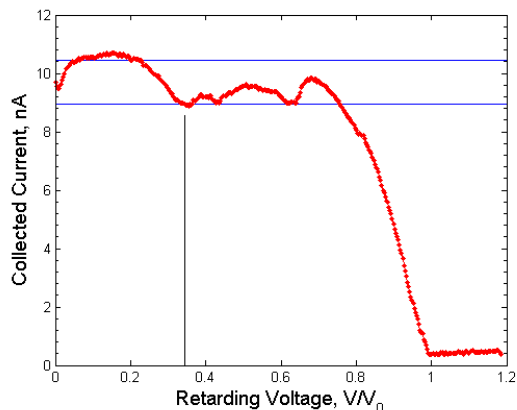


Figure 11. RPA for BMI-I (70° , 1600 V).

Unfortunately the results for EMI-BF<sub>4</sub>, a very well characterized ionic liquid in ILIS,<sup>1,5,6</sup> were anomalous. The RPA scans for EMI-BF<sub>4</sub> were far from monoenergetic and instead showed a large low energy current fraction and a large relative fraction of fragmented dimers in field-free space.<sup>3</sup> This may be due to the fact that the RPA was not well aligned with the source. The RPA was probably collecting only the edge of the ion beam, which likely has more low energy species than the beam center.<sup>3</sup>

An older set of RPA data for EMI-BF<sub>4</sub> was taken using the same source set up, needle, and RPA at the same voltages and temperatures.<sup>3</sup> The only difference was that the RPA period was 8 s rather than 5 s.<sup>3</sup> The RPA curves from the older dataset look much better than the anomalous ones, so they were processed using the same method as described in this section to determine the dimer fragmentation current fraction in field-free space. EMI-BF<sub>4</sub> was tested again is because the TOF data from the older dataset was of poor quality and needed to be repeated.<sup>3</sup>

The fraction of dimer fragmentation in field-free space does not vary strongly with the source potential, so for each liquid at a given temperature, it was averaged for all voltages.<sup>3</sup> Fig. 12 shows the current fraction of dimer fragmentation in field-free space at each temperature as a function of the number of atoms in the anion of the ionic liquid at 70°C. The positive mode is shown in a) and the negative mode is shown in b).

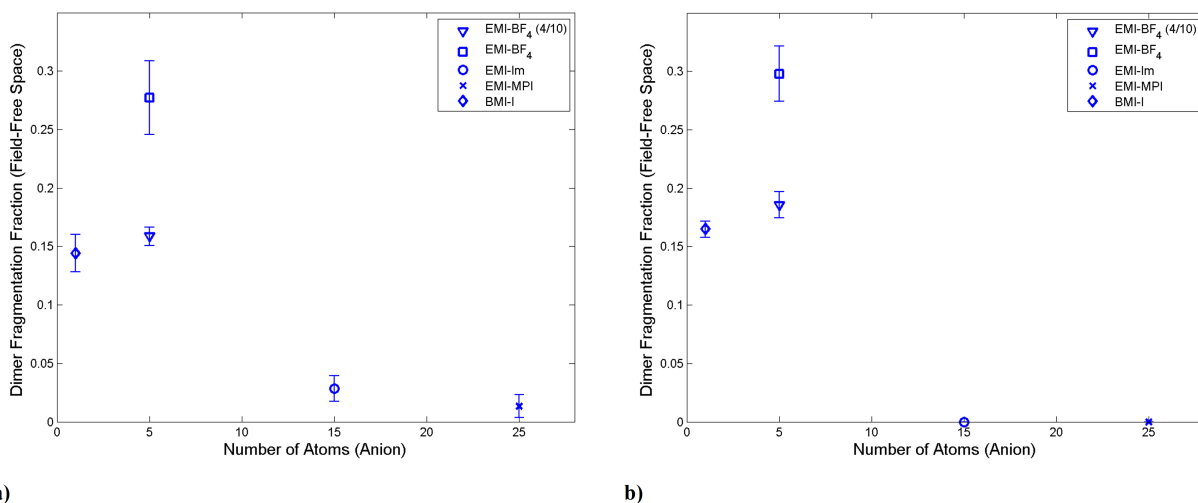


Figure 12. Dimer Fragmentation Fraction in Field-Free Space at 70°C: a) Positive Mode, b) Negative Mode.<sup>3</sup>

The error bars are the standard deviation from the mean. EMI-Im and EMI-MPI have the lowest current fraction of dimers that fragment in field-free space. The anomalous EMI-BF<sub>4</sub> dataset shows the highest fragmentation current fraction. Even the older dataset, labeled by the experiment date 4/10, shows a higher fragmentation current fraction than BMI-I. This trend was observed at the other temperatures.<sup>3</sup>

The current fraction of fragmented dimers in field-free space depends on the current fraction of dimers that can fragment in field-free space.<sup>3</sup> It was found that the current fraction of dimers that survive is not the same for all ionic liquids.<sup>3</sup> Therefore in order to evaluate the stability of dimers in field-free space, the fragmentation current fraction must be normalized by the survived dimer current fraction.<sup>3</sup> Using positive TOF data, the dimer fragmentation percentage in field-free space was estimated and is shown in Fig. 13 as a function of the number of atoms in the anion of the ionic liquid at 70°C.

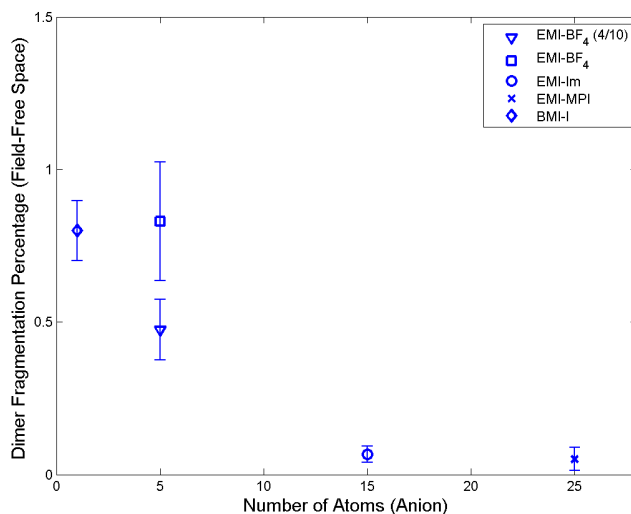


Figure 13. Dimer Fragmentation Percentage in Field-Free Space at 70°C (Positive Mode).<sup>3</sup>

Note that the old EMI-BF<sub>4</sub> RPA curves were normalized using TOF data from the newer EMI-BF<sub>4</sub> dataset since high quality TOF data was not available for the older dataset.<sup>3</sup> This is acceptable because the anomalous RPA data was likely a result of the RPA detector misalignment, which should not change the TOF results.<sup>3</sup> This was only done for the positive mode because negative TOF data was not available (see section V.b).

Fig. 13 shows that BMI-I has the highest dimer fragmentation percentage in field-free space. For the purposes of this discussion, the anomalous EMI-BF<sub>4</sub> data is ignored and instead the older, more reliable dataset is used. Finally EMI-Im and EMI-MPI have the lowest fragmentation percentages in field-free space. These results are in agreement with past observations and are in support of the hypothesis. However it is critical to stress that these results are not sufficient to validate the hypothesis. The full beam was not collected by the RPA detector, which means that angular variations in beam composition could impact the results.<sup>3</sup> Also, while combining the datasets helped determine a more reliable estimate of the fragmentation percentages for EMI-BF<sub>4</sub>, it is not good practice and is not a robust method for testing the hypothesis. See section VI for further discussion.

## B. Time of Flight Mass Spectrometry

Time of flight measurements were taken for all liquids in the positive mode at the same set of temperatures and voltages as for the RPA data. Measurements in the negative mode were not conducted due to a lack of a working amplifier. In the negative mode, the high voltage for the Channeltron is applied at the electron collector plate, which means that the amplifier circuitry must be protected from the high voltage.<sup>3</sup> Some measurements were made in the negative mode for EMI-BF<sub>4</sub>, but the amplifier failed while testing other liquids.<sup>3</sup> Measurements for the negative mode will be made in future work.

The TOF scans for each voltage and temperature were averaged 4096 times on the oscilloscope over the period of a few minutes.<sup>3</sup> The beam composition and current fraction due to dimer fragmentation in the acceleration region can be easily measured from the TOF spectra. Fig. 14 shows the time of flight signal for BMI-I at 70° and 1650 V. The monomers, dimers, and fragmented dimers are labeled.

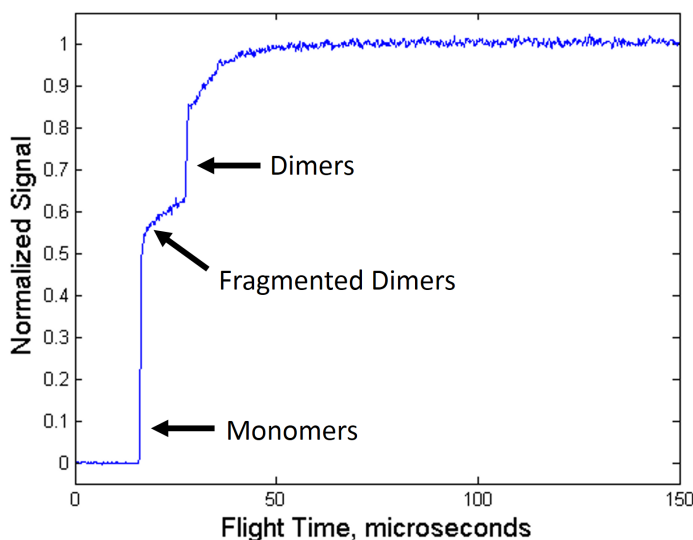
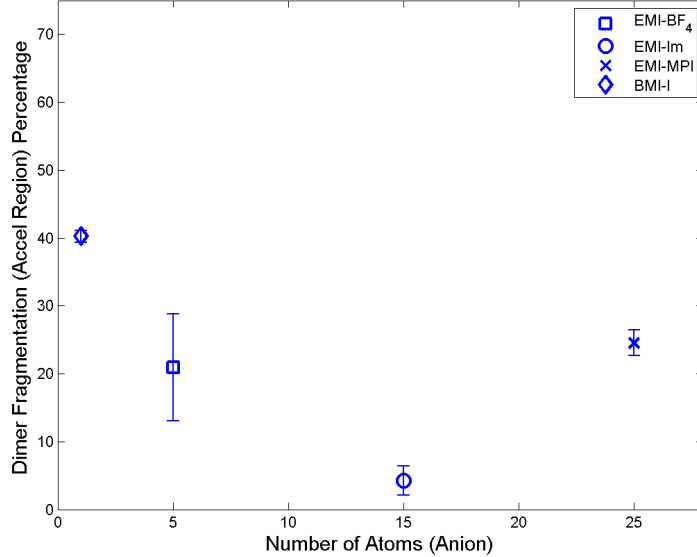


Figure 14. TOF for BMI-I (70°, 1650 V).

To evaluate the stability of a positive dimer of a given liquid, the ratio of the fragmented dimer current fraction to the total current fraction of dimers is used.<sup>3</sup> The total current fraction of dimers includes both the fragmented dimers and the dimers that survive break up in the acceleration region.<sup>3</sup> For each liquid at each temperature, this quantity was averaged over the same narrow voltage band (50 - 100 V in width).<sup>3</sup> Fig. 15 shows the percent fragmentation of dimers in the acceleration region as a function of the number of atoms in an anion at 70°C.



**Figure 15. Dimer Fragmentation Fraction in the Acceleration Region at 70° (1400 - 1450V).<sup>3</sup>**

Except for EMI-MPI, the TOF results support the hypothesis. The dimer fragmentation fraction for other temperatures shows the same trend as in Fig. 15.<sup>3</sup> BMI-I has a higher dimer fragmentation percentage than EMI-BF<sub>4</sub>, and EMI-BF<sub>4</sub> has a higher dimer fragmentation percentage than EMI-Im. The TOF detector only samples a small solid angle of the beam, which is a critical limitation for interpreting the results.<sup>3</sup> If the beam is off axis, the detector could be sampling the fringe of the beam instead of the center. Past experiments with this detector indicate that the beam composition is not angularly uniform, which means that the relative fragmentation percentage could vary across the beam.<sup>3</sup> High quality, full-beam RPA measurements could be used to check if the small solid angle of the beam that the TOF detector measures is representative of the full beam.<sup>3</sup> This will be the goal of future work.

## VI. Conclusion

Fragmentation of solvated species in ILIS beams has an important effect on the propulsive efficiency of ion electrospray thrusters, which motivates its study. Past experiments show that different ionic liquids show different amounts of fragmentation.<sup>2</sup> It is hypothesized that fragmentation decreases with increasing molecular complexity, or the number of atoms, of the ionic liquid.<sup>2</sup> This work was motivated by the need for the characterization of different ionic liquids under the same conditions. Retarding potential analyzer and time of flight mass spectrometry measurements were made over a range of ionic liquid temperatures and source potentials for four different ionic liquids. The retarding potential analyzer measurements yielded the current fraction of dimers that fragment into monomers in field-free space.<sup>3</sup> The time of flight measurements yielded the fraction of dimers that fragment into monomers inside of the acceleration region.<sup>3</sup> With a few exceptions, the TOF and RPA measurements support the past observations and the hypothesis. The exceptions may or may not be explained by the limitations of both detectors.<sup>3</sup> This work is not sufficient to determine the validity of the hypothesis, thus future study is required.<sup>3</sup>

Future work includes the improvement of the detectors. A new RPA detector will be built in order to make high quality full-beam measurements. The RPA will be placed farther away from the source in order to enhance the steps that correspond to fragmentation in field-free space.<sup>3</sup> The RPA will be made large enough to collect the full current of the beam, which will allow for stronger conclusions to be made from the data.<sup>3</sup> The RPA in this work only collects a fraction of the beam, which means that the angular dependence of the beam composition is a concern for interpreting the results.<sup>3</sup> With a full-beam RPA, there will not be a discrepancy in the results from a slightly off-axis ion beam.<sup>3</sup> Finally the new RPA will likely have a spherical geometry, which will significantly reduce beam spreading features.<sup>6</sup> This is especially important when trying

to study the population of ions that have energies slightly less than the source potential; these ions come from fragmentation almost immediately after emission.<sup>3</sup>

The time of flight detector will be used to study the angular dependence of the beam composition to determine how strongly this could affect the results.<sup>3</sup> Deflector plates can be used to deflect the beam and control what regions of the beam the TOF detector samples.<sup>3</sup> Additionally the TOF spectra can be used to generate the energy distribution of the ion beam.<sup>3</sup> The flight times of fragmented species yield the energy of the ions by assuming that the fragmented ion comes from a specific type of fragmentation event (eg. dimer into monomer).<sup>3</sup> If the energy distribution from the TOF data compares well with the RPA data, then the TOF results can be used with more confidence. Once the RPA and TOF detectors are well-characterized and yield more reliable data, a wider sample of ionic liquids will be tested. This will allow for the validity of the hypothesis to be evaluated with more certainty.

## Acknowledgments

This research was supported by the National Aeronautics and Space Administration and the Department of Defense.

## References

<sup>1</sup>Lozano, P., and Martinez-Sanchez, M. "Ionic liquid ion sources: characterization of externally wetted emitters," *Journal Of Colloid And Interface Science*, Vol. 282, No. 2, 2005, pp. 415-421.

<sup>2</sup>Coles, T., and Lozano, P. "Investigating efficiency losses from solvated ion fragmentation in electrospray thruster beams," *49th AIAA/ASME/SAE/ASEE Joint Propulsion Conference*, AIAA-2013-4033, 2013.

<sup>3</sup>Miller, C. "On the Stability of Complex Ions in Ionic Liquid Ion Sources," Masters Thesis, Aeronautics and Astronautics Dept., Massachusetts Institute of Technology, Cambridge, MA, 2015 (submitted).

<sup>4</sup>Taylor, G. "Disintegration of Water Drops in an Electric Field," *Proceedings of the Royal Society of London*, Vol. 280, No. 1382, 1964, pp. 383-397.

<sup>5</sup>Romero-Sanz, I., Bocanegra, R., Fernandez de la Mora, J. F., and Gamero-Castano, M. "Source of heavy molecular ions based on Taylor cones of ionic liquids operating in the pure ion evaporation regime," *Journal Of Applied Physics*, Vol. 94, No. 5, 2003, pp. 3599-3605.

<sup>6</sup>Coles, T., Fedkiw, T., and Lozano, P. "Investigating ion fragmentation in electrospray thruster beams," *48th AIAA/ASME/SAE/ASEE Joint Propulsion Conference*, AIAA-2012-3793, 2012.

<sup>7</sup>Lozano, P., and Martinez-Sanchez, M. "Efficiency estimation of EMI-BF<sub>4</sub> ionic liquid electrospray thrusters," *41st AIAA/ASME/SAE/ASEE Joint Propulsion Conference and Exhibit*, AIAA-2005-4388, 2005.

<sup>8</sup>Lozano, P. "Energy properties of an EMI-Im ionic liquid ion source," *Journal Of Physics D-Applied Physics*, Vol. 39, No. 1, 2006, pp. 126, 134.

<sup>9</sup>Coles, T. "Investigating efficiency losses from solvated ion fragmentation in electrospray thruster beams," *49th AIAA/ASME/SAE/ASEE Joint Propulsion Conference*, 2013, PowerPoint presentation.

<sup>10</sup>Fedkiw, T., and Lozano, P. "Development and characterization of an iodine field emission ion source for focused ion beam applications," *Journal Of Vacuum Science & Technology: Part B-Microelectronics & Nanometer Structures*, Vol. 27, No. 6, 2009, pp. 2648-2653.